Relevance-based Channel Selection for EEG Source Reconstruction: An Approach to Identify Low-density Channel Subsets

Andres Soler[1], Eduardo Giraldo[2], Lars Lundheim[3] and Marta Molinas[1]
[1]*Department of Engineering Cybernetics, Norwegian University of Science and Technology, Trondheim, Norway*
[2]*Department of Electrical Engineering, Universidad Tecnológica de Pereira, Pereira, Colombia*
[3]*Department of Electronic Systems, Norwegian University of Science and Technology, Trondheim, Norway*

Keywords: Relevance Channel Selection, Low-density EEG, EEG Signals, Source Reconstruction.

Abstract: Electroencephalography (EEG) Source Reconstruction is the estimation of the underlying neural activity at cortical areas. Currently, the most accurate estimations are done by combining the information registered by high-density sets of electrodes distributed over the scalp, with realistic head models that encode the morphology and conduction properties of different head tissues. However, the use of high-density EEG can be unpractical due to the large number of electrodes to set up, and it might not be required in all the EEG applications. In this study, we applied relevance criteria for selecting relevant channels to identify low-density subsets of electrodes that can be used to reconstruct the neural activity on given brain areas, while maintaining the reconstruction quality of a high-density system. We compare the performance of the proposed relevance-based selection with multiple high- and low-density montages based on standard montages and coverage during the reconstruction process of multiple sources and areas. We assessed several source reconstruction algorithms and concluded that the localization accuracy and waveform of reconstructed sources with subsets of 6 and 9 relevant channels can be comparable with reconstructions done with a distributed set of 128 channels, and better than 62 channels distributed in standard 10-10 positions.

1 INTRODUCTION

Since the first report of human EEG recordings done by Hans Berger in 1929 (O'Leary, 1970). The EEG signals have been considered a window to the human brain and their analysis as a powerful tool to understand the multiple brain processes. EEG signals can be used to estimate the properties of the underlying brain activity, generally its localization and waveform, this process is often referred to as source reconstruction (Phillips et al., 1997). The accurate reconstruction of the brain activity requires solving the forward and inverse problems. Briefly, the forward problem solution consists of modelling the interaction between a large population of neurons at the brain cortex and the electrical field that is recorded. Multiple methods, like Finite Element Modelling (FEM) and Boundary Element Modelling (BEM) based on Magnetic resonance imaging (MRI) head images allow to obtain realistic representations of the brain and the accurate modelling of source-electrode interaction (Hallez et al., 2007). In contrast, the inverse problem solution is the estimation of the brain activity properties by using the information registered by the electrodes and the forward model solution (Michel and Brunet, 2019).

The number of electrodes plays a key role in source reconstruction and it is a well established fact that a high number of electrodes allows obtaining a better estimation of the source activity. However, the EEG electrode distribution was mostly conceived based on coverage and not based on their contribution to accuracy. With a wide coverage is possible to attain a better overview of the brain activity over the entire head, and compare it between both hemispheres to obtain lateralized information. In 1958, the 10-20 electrode positioning systems was introduced to facilitate the standardization of EEG recordings and benefit the comparison of findings in the scientific community (Jasper, 1958; Ten, 1961). Years afterwards, the 10-10 electrode positioning system (Chatrian et al., 1985) was presented as an inherent extension of the 10-20 system, which allowed covering the scalp with more electrodes. In 2001 this electrode layout was extended by the introduction of the 10-5 system (five percent electrode system for high-resolution EEG) (Oosten-

Soler, A., Giraldo, E., Lundheim, L. and Molinas, M.
Relevance-based Channel Selection for EEG Source Reconstruction: An Approach to Identify Low-density Channel Subsets.
DOI: 10.5220/0010907100003123
In *Proceedings of the 15th International Joint Conference on Biomedical Engineering Systems and Technologies (BIOSTEC 2022) - Volume 2: BIOIMAGING*, pages 174-183
ISBN: 978-989-758-552-4; ISSN: 2184-4305

veld and Praamstra, 2001), for which an extended nomenclature and location for up to 345 channels was proposed. However, the 10-5 electrode positioning system is not the only scalp distribution to reach hundreds of channels; other electrode distributions like the radial (BioSemi BV, Amsterdam, Netherlands), and geodesic (Electrical Geodesics, Inc., USA) allow recordings with up to 256 channels.

At the time of the introduction of the 10-5 system, it was known that the inverse solution required a higher number of electrodes to obtain more reliable reconstructions (Phillips et al., 1997). The number of channels for source reconstruction has been investigated in (Song et al., 2015; Sohrabpour et al., 2015). It has been proven that the use of high-density EEG systems favors the localization of brain sources compared to low-density ones. Particularly in (Sohrabpour et al., 2015) the authors presented a study with epileptic patients, where it was concluded that adding electrodes improves the accuracy. However, continuing to add channels beyond a certain point did not significantly improve the localization accuracy and which starts plateauing at that point. There is not a written consensus of what is and what is not high-density EEG, however, in (Seeck et al., 2017) it was suggested that high-density EEG can be considered between 64 to-256 channels. It is generally accepted that systems with 60 or more electrodes can be regarded as high-density EEG, while systems with 32 or below might be considered low-density EEG.

Some authors have investigated whether low-density arrays can accurately localize brain sources, (Jatoi and Kamel, 2018), where localization errors around 14 mm were obtained by using Multiple Sparse Priors (MSP) with a low-density montage of 7 electrodes. (Soler et al., 2020b) applied preprocessing with frequency decomposition techniques to improve source reconstruction with low-density electrodes arrays of 32, 16, and 8 channels. However, the aforementioned studies do not provide a rational criterion for selecting which electrodes will best contribute to accuracy from the considered EEG coverage.

In this study, we investigate the use of a data-driven relevance-based selection criteria for EEG channels to obtain low-density subsets to be considered during source reconstruction. Starting from high-density electrode layouts, we investigate the effect of reducing electrodes based on coverage, the use of the standard electrode montages, and our proposal based on relevance. Finally, we compare the reconstruction quality in terms of localization accuracy and correlation of the source activity, and provide a discussion over the results and the significance of using low-density electrode arrays in source reconstruction.

2 MATERIAL AND METHODS

2.1 Forward Modelling

EEG is an indirect measurement of the post-synaptic activity that takes place in the cortical areas; thousands of neurons should fire in synchrony to be able to obtain a measurable electric field at the scalp. It is because the local field potentials produced by extracellular currents of a large population of neurons (sources) propagate through different tissues attenuating their strength before reaching the scalp. The forward modelling is the representation of the relationship between the source activity and the electrical potential that can be measured by electrodes at the scalp. To accurately represent such complex relationships, the forward modelling considers the different head tissues and the flow of the electrical field across them.

To obtain accurate and realistic representations of this relationship, FEM and BEM methods combine tissue segmented MRI head images and the conductivity of the head tissues. The measured EEG can be represented theoretically using the forward equation in eq. 1. Where $\boldsymbol{M}$ is the forward model (also know as lead field matrix) with dimensions n by s (being n the number of channels and s the number of distributed sources), $\boldsymbol{y}$ with dimensions n by t (being t the number of samples) represents the electrodes measurement of the electric potential generated by the source activity in the cortical areas represented by $\boldsymbol{x}$, with dimensions s by t . ε represents the noise usually presented in the measurements.

$$\boldsymbol{y} = \boldsymbol{M}\boldsymbol{x} + \varepsilon \tag{1}$$

2.2 Inverse Modelling

In contrast to the forward problem, the inverse problem is the estimation of the source activity from the recorded signals, it is also known as source reconstruction. In the solution of the inverse problem, the lead-field matrix $\boldsymbol{M}$ is known, as it establishes a set of distributed sources over all the cortical areas. The inverse solution is the estimation of the contribution of each source to the recorded EEG. The inverse problem is characterized to be mathematically ill-posed and ill-conditioned ((Hämäläinen and Ilmoniemi, 1994)). It is because the volume of the information available in the EEG recording comes from hundreds of electrodes, in the best cases; a number

which is much lower than the number of unknowns, usually thousands of sources.

Multiple methods based on Tikhonov regularization have been applied to overcome these challenges. Some of the most known and used methods based on regularization are the minimum norm estimation (MNE) (Hämäläinen and Ilmoniemi, 1994), its weighted version (wMNE) (Iwaki and Ueno, 1998; Pascual-Marqui, 2002) to compensate for deep activity, and the standardized low-resolution tomography (sLORETA), which is characterized by the zero error localization in absence of noise ((Pascual-Marqui, 2002)). From another perspective, the multiple signal classification (MUSIC) (Mosher and Leahy, 1998) algorithm estimates the localization of a source by identifying the contribution of each source when testing whether its projection (topography) belongs to a signal-subspace or noise-subspace. This particular algorithm is useful to identify the number of active sources and locate them. However, the contribution is calculated using a localizer function, and it is often difficult to identify the true active sources due to the fact that neighbour sources of the true source can lead to a similar topography and similar value in the localizer function. Therefore, to avoid this problem the topography is out-projected and the sources can be calculated one by one in recursive applied MUSIC (RAP-MUSIC). However, the RAP version has an undesired property of leaving large values in the localizer function in the vicinity of already located sources, which produces an overestimation of the number of sources due to some false positive sources. This weakness was improved by applying a sequential dimension reduction of the estimated remaining signal space at each recursion step in the truncated RAP-MUSIC (TRAP-MUSIC) (Mäkelä et al., 2018; Ilmoniemi and Sarvas, 2019). When the localization of the source is estimated by a MUSIC-based algorithm, the source time-course can be estimated using Tikhonov regularization, by constraining the solution to the previous estimated locations.

In this study, we considered five methods for source reconstruction, wMNE, sLORETA, MUSIC, TRAP-MUSIC, and Multiple Sparse Priors (MSP). This method is characterized for offering a low free-energy solution (Friston et al., 2008) and has been investigated over low-density EEG settings in (Jatoi et al., 2014).

We used the "New York Head Model" as the forward model (Huang et al., 2016). It is a six-layer FEM model that considered the conductivity of the scalp, skull, CSF, gray matter, white matter, and air cavities. The model relates 231 channels with a multiple number of sources $75K$, $10K$, $5K$, and $2K$. The lead field matrix of $10K$ sources was used to generate synthetic EEG signals with known ground-truth source activity (see section 2.3) and the lead field matrix of $5K$ sources was used for inversion, to prevent the so-called inverse crime (Colton and Kress, 2019).

2.3 Ground-truth EEG Dataset

A set of three sources with temporal mixing was simulated at different frequencies. Using the following equation:

$$x_i(t_k) = e^{-\frac{1}{2}\left(\frac{t_k - c_i}{\sigma}\right)^2} sin(2\pi f_i t_k) \quad (2)$$

Each source number i is a Gaussian windowed sinusoidal activity and has an associated frequency f_i, time center c_i, a Gaussian window width σ_i, and a location loc_i in a predefined region of the brain. A similar scheme of simulation was used in (Soler et al., 2020b; Soler et al., 2020a). The parameters for each source are presented in table 1.

Table 1: Parameters for source simulation.

s_i	i=1	i=2	i=3
f_i (Hz)	19	10	7
c_i (s)	0.5	1.0	1.5
sigma_i	0.12	0.12	0.12
loc_i	Occipital lobe	Sensory-motor cortex	Frontal lobe

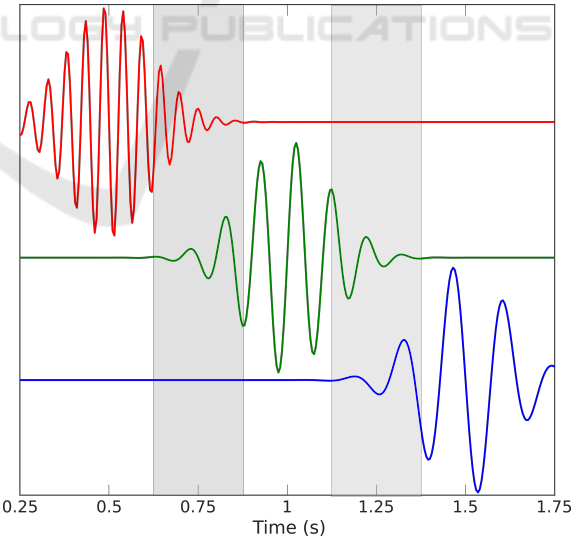

Figure 1: Example of the time-courses of simulated source activity. The light-gray shapes show the time windows where temporal mixing is present between the sources. Sources s_1, s_2, and s_3 are depicted in red, green, and blue color, respectively.

Although the sources have a predefined region of the brain, the final locations of the sources were

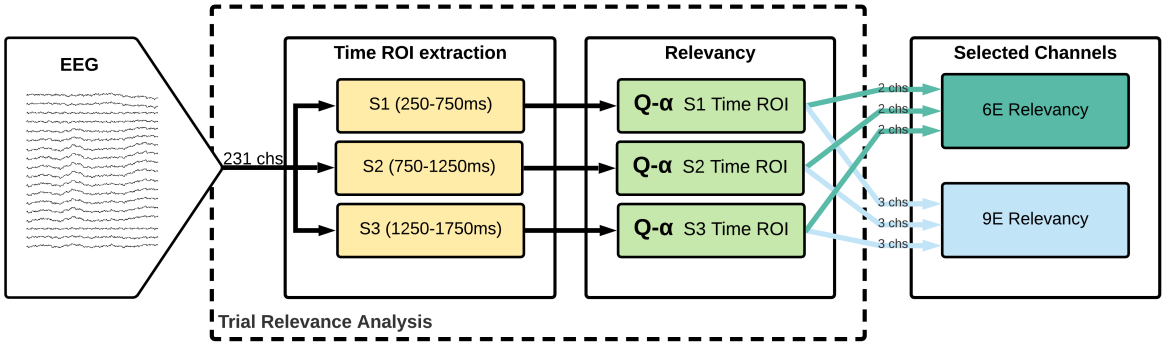

Figure 2: Relevance channel selection procedure for selecting the 6 and 9 most relevant channels per each EEG trial.

randomly selected from a set of twelve locations in each area, distributed equally for each hemisphere. The source ground-truth simulation process was repeated to obtain 150 trials with different combination of source locations. The synthetic EEG was obtained by using the forward equation (eq. 1), a signal-to-noise ratio (SNR) of $0dB$ was added to simulate the level of noise typically found in event related potentials ERPs. An example of the ground-truth activity can be seen in figure 1

2.4 Relevance based Channel Selection

We applied the relevance analysis proposed by (Wolf and Shashua, 2005), to select k most relevant EEG channels to be used for source reconstruction. A time-ROI is selected for each source, and then for each time-ROI, the relevance for each channel is calculated using the Standard Power-Embedded Q-α algorithm. As three sources were simulated, the $k = 2$ and $k = 3$ most relevant channels per each source time-ROI were selected, therefore, the total of electrodes per EEG used during source reconstruction for $k = 2$ and $k = 3$ were 6 (we refer as $Rel-6E$) and 9 (we refer as $Rel-9E$) respectively. In figure 2 is summarized the selection process and presented the Time-ROI times for each source.

By using the Standard Power-Embedded Q-α algorithm, it is calculated a relevance indicator associated with each channel, this indicator is represented by $\boldsymbol{\alpha} \in \mathbb{R}(0,1)$, where the values closer to 1 represent the most relevant channels. (Wolf and Shashua, 2005) presented the algorithm for feature selection, being relevance directly related to the clustering quality of features. Here, applied to EEG channel selection, the relevance measures the ability of the channels to capture the underlying neural activity in the time-ROI. Here the algorithm is presented in the context of EEG channel selection. Consider the pre-processed EEG as $\boldsymbol{y}_1^T, ..., \boldsymbol{y}_n^T$, such that each row is centered around zero and its L2 norm $||\boldsymbol{y}_i|| = 1$. For notation, the term P^T stands for the transpose of matrix P. Consider $\boldsymbol{A}_\alpha$ to be the affinity matrix of the inner-product between data points weighted by $\boldsymbol{\alpha}$ as $\boldsymbol{A}_\alpha = \sum_{i=1}^{n} \boldsymbol{\alpha}_i \boldsymbol{y}_i \boldsymbol{y}_i^T$. Also consider $\boldsymbol{Q}$ as an orthonormal t by k matrix, whose columns are the k eigenvectors of $\boldsymbol{A}$ associated with the highest eigenvalues. To find the channel relevance α is calculated by solving the optimization problem presented below:

$$\begin{aligned} &\max_{\boldsymbol{Q},\boldsymbol{\alpha}} \quad trace \quad (\boldsymbol{Q}^T \boldsymbol{A}_\alpha^T \boldsymbol{A}_\alpha \boldsymbol{Q}) \\ &\text{subject to} \quad \boldsymbol{\alpha}^T \boldsymbol{\alpha} = 1 \end{aligned} \tag{3}$$

which can be solved by applying the Power-Embedded Q-α algorithm (algorithm 1) adapted for EEG channel relevance. The number of r iterations was set to $r = 10$ according to the number of iterations suggested in (Wolf and Shashua, 2005).

Algorithm 1: Power-Embedded Q-α algorithm.

procedure Q-α(y)
  $Q_0 \leftarrow$ random orthonormal q by k matrix
  $r \leftarrow 1$
  while $r \leq 10$ **do**
    $G_{i,j} \leftarrow (\boldsymbol{y}_i^T \boldsymbol{y}_j) \boldsymbol{y}_i^T \boldsymbol{Q}_{r-1} \boldsymbol{Q}_{r-1}^T \boldsymbol{y}_j$
    $\boldsymbol{\alpha} \leftarrow$ the largest eigenvector of G
    $\boldsymbol{A}_\alpha \leftarrow \sum_{i=1}^{n} \boldsymbol{\alpha}_i \boldsymbol{y}_i \boldsymbol{y}_i^T$
    $Z \leftarrow \boldsymbol{A}_\alpha \boldsymbol{Q}_{r-1}$
    $\boldsymbol{Q}_r R \leftarrow$ QR decomposition of Z
    $r \leftarrow r + 1$
  end while
  return α
end procedure

2.5 Standard-based and Coverage-based Channel Distributions

The New York Head forward model in (Huang et al., 2016) considers 231 electrodes positions, of which 161 are located in the scalp according to the 10-5

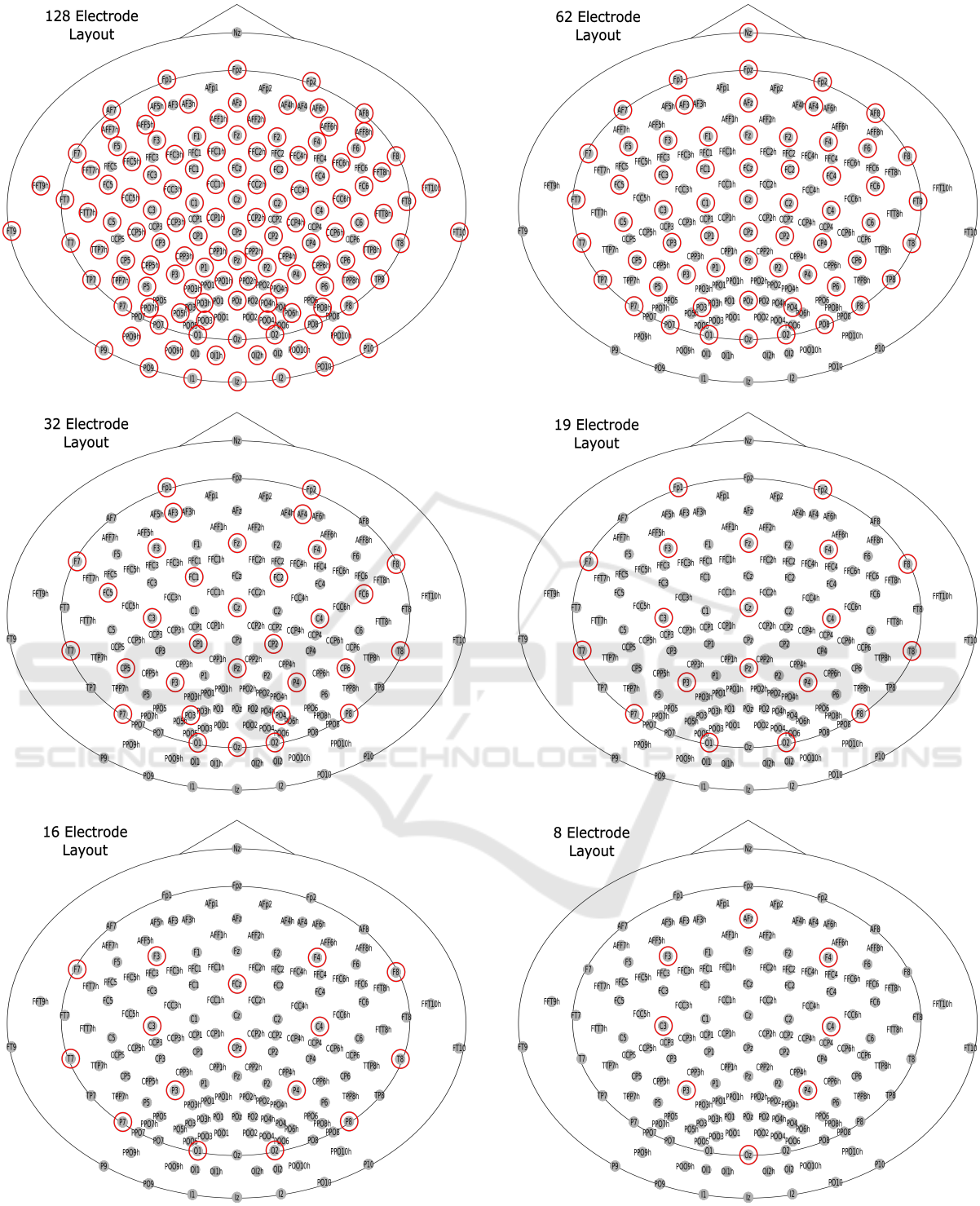

Figure 3: Standard-based (top row) and coverage-based (middle and bottom rows) electrode Layouts. The selected electrodes for each layout are marked with a red circle over the 161 electrodes available in the New York Head.

system, and 70 electrodes distributed between neck and face. To compare the performance of source reconstruction using relevance-based channel selection, we selected multiple layouts based on coverage and standard systems. One of the selected electrode distribution is based on the 161 scalp electrodes of the

model, we refer to it as $HD-161E$. Two subsets of 19 and 62 electrodes were considered based on the 10-20 and 10-10 standard electrode distribution, we refer to them as $LD-19E(10-20)$ and $HD-62E(10-10)$, respectively. Four more subsets of electrodes were selected based on coverage criteria, one lays in the category of high-density with 128 channels, it is referred as $HD-128E$; the other three are considered low-density, with channel numbers of 32, 16, and 8, they were selected trying to keep an equal coverage of the head, they are referred as $LD-32E$, $LD-16E$, and $LD-8E$. The Figure 3. shows the different standard-based and coverage-based layouts.

2.6 Evaluation Procedure

The evaluation procedure is presented in figure 4. It starts with the generation of the ground-truth EEG dataset (section 2.3). The 150 trials are processed separately, for each EEG, the channels are selected according to the three criteria: coverage-based, standard-based, and relevance-based. The selected channels are considered during inverse solution and processed with the five source reconstruction algorithms. The algorithms wMNE, sLORETA, and MSP provide localization and time-course of the sources, while MUSIC and TRAP-MUSIC provided only source localization, however, they can be complemented with Tikhonov regularization constrained to the estimated locations to estimate the time-course activity.

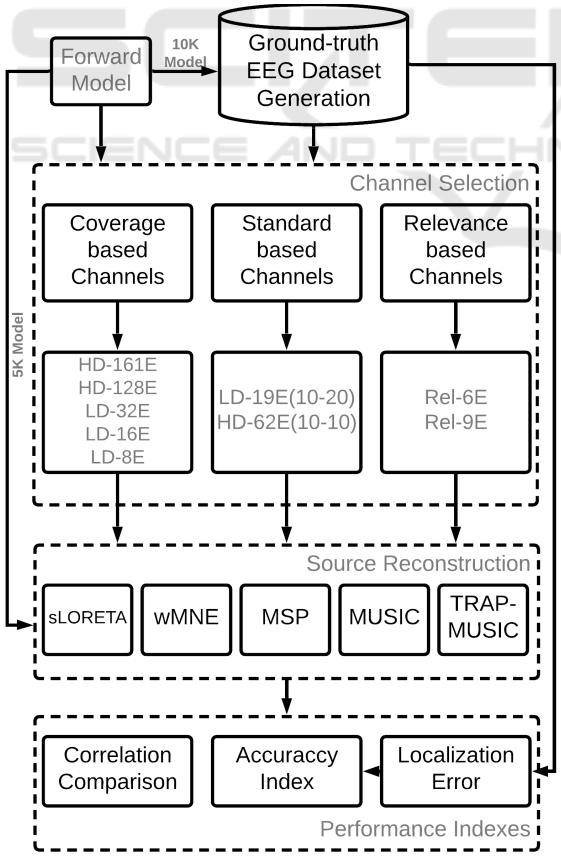

Figure 4: Summary of the evaluation procedure.

After estimating the brain activity, the localization error for each of the three sources is calculated by using the euclidean distance (equation 4) between the ground-truth P_x and the estimated $P_{\hat{x}}$ location. Then, the localization error is averaged between the three sources to provide a single value for the error of localization.

$$LocE = ||P_x - P_{\hat{x}}||_2 \tag{4}$$

The number of trials in which the localization error with relevance selection was equal or lower than with coverage or with standard-based layouts is proposed to measure at what extend of trials, the relevance selection produced equal or better accuracy compared to the other criteria. We refer to it as the Accuracy Comparison index.

The time course of the sources reconstructed with $Rel-6E$, $Rel-9E$ are extracted and compared with the time courses reconstructed with the denser electrode layout $HD-161E$. To compare them, we used the Pearson Correlation Coefficient:

$$r = \frac{\sum(x_{1i}-\bar{x}_{1i})(x_{2j}-\bar{x}_{2j})}{\sqrt{\sum(x_{1i}-\bar{x}_{1i})^2\sum(x_{2j}-\bar{x}_{2j})^2}} \tag{5}$$

where i and j are the location of the sources with the highest amplitudes of two different reconstructions, and x_{1i} and x_{2j} are the time courses.

3 RESULTS

The mean and standard deviation of the localization error for the 150 trials is shown in figure 5. The electrode layouts in the x-axis were organized according to the number of electrodes they consider, excepting the $Rel-6E$ and $Rel-9E$ that were located first on the left side. The best accuracy was obtained when using the highest number of electrodes with the $HD-161E$ layout when considering all the scalp electrodes of the forward model. In contrast, the worst accuracy was obtained when using the $LD-8E$ layout. A trend can be seen in the localization error, as the number of electrodes is being reduced, the localization accuracy decreases. However, the trend is abruptly interrupted when considering the results of the channels selected with the relevance criteria.

The localization error of the relevance selection $Rel-6E$ and $Rel-9E$ are comparable to the $HD-128E$ test. Particularly the methods wMNE,

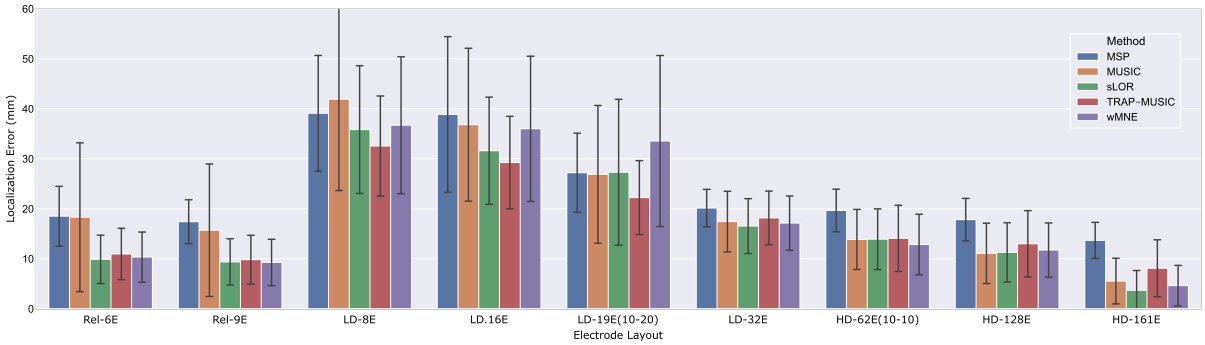

Figure 5: Localization error of the multiple electrode layouts combined with each of the source reconstruction algorithms.

sLORETA, and TRAP-MUSIC, for the relevance cases offer a slightly better localization error mean with similar standard deviation as with the $HD-128E$. Here it is remarkable that for the same methods, $Rel-9E$ kept the mean localization error below 10mm, result that was achieved only with all the electrodes $HD-161$ case. The case of the MSP method presents a similar behavior with $Rel-9E$ compared to $HD-128E$, and the MSP accuracy with $Rel-9E$ was slightly lower than with $HD-128E$. In contrast, the MUSIC method was highly affected by the reduction in the number of electrodes. It is a generalized effect for this particular algorithm, regardless of whether the channels were selected with relevance or not; as the number of electrodes is reduced the standard deviation increases.

Table 2. offers the accuracy comparison indexes when considering the percentage of trials that obtained equal or better localization error with relevance criteria $Rel-6E$ and $Rel-9E$, than the other layouts based on standard and coverage criteria. It is remarkable that for methods sLOR, wMNE, and TRAP-MUSIC, $Rel-9E$ obtained an index between 61% and 68% when comparing with $HD-128E$ and between 67% and 73% when comparing with $HD-62E(10-10)$, especially considering that $Rel-9E$ has 119 and 51 fewer channels than $HD-128E$, and $HD-62E$ respectively. In the case of $Rel-6E$ the results are also noticeable, it uses 122 fewer channels than $HD-128E$ and 55 less than $HD-62E(10-10)$, and it obtained indexes between 59% and 64% when comparing with $HD-128E$ and between 63% and 71% when comparing with $HD-62E(10-10)$.

To compare the reconstructed time courses of the estimated source activity, we computed the Pearson correlation coefficient between the reconstructions using $Rel-6E$ and $Rel-9E$ and the denser electrode layouts of $HD-161E$ and $HD-128E$. The comparison was done for the reconstructions with the methods that obtained the lowest localization error, sLORETA, and wMNE. The results of the comparison between

Table 2: Accuracy Comparison Index, percentage of trials that obtained equal or better localization error when comparing the relevance criteria $Rel-6E$ and $Rel-9E$ with other electrode configurations.

Methods	Channel Layout	Rel-6E	Rel-9E
sLOR	LD-8E	0,96	0,97
	LD-16E	0,95	0,95
	LD-19E	0,91	0,92
	LD-32E	0,77	0,85
	HD-62E	0,71	0,73
	HD-128E	0,59	0,61
	HD-161E	0,11	0,11
WMN	LD-8E	0,97	0,97
	LD-16E	0,95	0,97
	LD-19E	0,93	0,94
	LD-32E	0,79	0,84
	HD-62E	0,63	0,67
	HD-128E	0,62	0,68
	HD-161E	0,19	0,21
MSP	LD-8E	0,91	0,97
	LD-16E	0,90	0,94
	LD-19E	0,75	0,80
	LD-32E	0,67	0,70
	HD-62E	0,57	0,64
	HD-128E	0,49	0,53
	HD-161E	0,21	0,22
MUSIC	LD-8E	0,82	0,88
	LD-16E	0,83	0,89
	LD-19E	0,75	0,79
	LD-32E	0,62	0,68
	HD-62E	0,47	0,55
	HD-128E	0,42	0,47
	HD-161E	0,13	0,15
TRAP-MUSIC	LD-8E	0,96	0,97
	LD-16E	0,96	0,95
	LD-19E	0,89	0,87
	LD-32E	0,81	0,88
	HD-62E	0,65	0,69
	HD-128E	0,64	0,63
	HD-161E	0,32	0,41

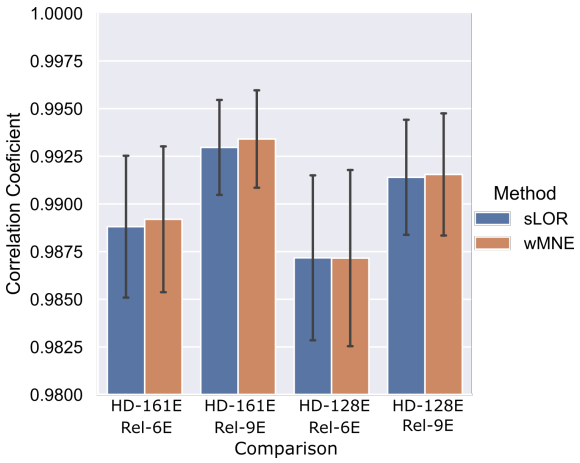

Figure 6: Source time courses correlation coefficient between high-density layouts and relevance based channel selection.

the aforementioned sets of channels are presented in figure 6. It can be seen that the correlation in all the cases was more than 98% and particularly for the comparisons with $Rel-9E$, the correlation values were higher than 99%.

To offer an overview of the relevance-based selected channels we computed the number of times that the channels were repeatedly chosen by the two relevance criteria. The number of repetitions for each channel is shown in figure 7. For relevance analysis, the 231 channels positions of the forward model were considered, including 70 locations in face and neck, however, none of the selected channels were in those areas. It is important to note that the selected channels across trials were distributed between both hemispheres, in which a particular position in the right hemisphere and its equivalent at the left hemisphere obtained similar repetition values. The small differences can be explained by the location of the simulated sources which were selected randomly from a pre-set of sources for each brain area, equally distributed between both hemispheres.

4 DISCUSSION AND CONCLUSIONS

With the introduction of relevance criteria for channel selection, a subset of selected channels, with a sparser number far from high-density EEG, can reconstruct a set of sources in the brain with comparable quality as a high-density number of channels. The reconstruction quality obtained with relevance channel selection can be comparable to using a set of 128 channels, and better than 62 channels in terms of the localization error. Moreover, in terms of the time-courses similarity, the high level of correlation obtained between the reconstruction with the relevant channels and the densest coverage-based layouts supports the hypothesis that relevance-based channel selection criteria can be comparable with high-density to reconstruct a particular brain activity.

The aim of this work is not to discourage the use of high-density EEG systems, it is rather to offer an alternative technique to select and reduce the number of electrodes for source reconstruction while keeping the quality. In situations where for practical reasons high-density systems are not applicable or affordable, low-density EEG solutions designed with relevance criteria will favour portability and reduce the volume of data while achieving the same quality as the high density solutions. These traits will enable the development of much needed EEG tools for medical diagnosis and non-medical applications. The results of this research suggest the application of this analysis in cases in which apriori known areas of the brain are going to be monitored and it is not possible or difficult to constantly measure with a high-density system. For example, in Brain-computer interfaces (BCI) systems based on source reconstructed activity (Edelman et al., 2016; Lindgren, 2017) or Mobile Brain Imaging (MoBI) applications in which the recordings are taken out of the lab (Gramann et al., 2011; Lau-Zhu et al., 2019).

It is important to consider that the selected electrodes based on relevance criteria are relevant on the basis of the particular source activity in which the analysis is applied. It must not be miss-interpreted that a selected set of electrodes can be used for mapping all the cortical regions. In such cases, to estimate a generalized activity over the brain, high-density is proven to be effective regardless of the area of the brain activity.

It is important to note that multiple channels that were repeatedly selected were located in positions out of standards 10-10, and 10-20, which supports the idea that multiple locations in non-standard positions contribute to improving the reconstruction quality, unfortunately, these positions are generally available only in denser layouts and EEG caps. However, the use of head models including intermediate positions can be combined with the physical adjustment of the positions of the electrodes of a system to the relevant selected ones, in order to monitor a particular brain activity.

The proposed relevance-based channel selection for source reconstruction remains to be verified over real signals, further studies on multiple recording paradigms and analysis of different brain activity re-

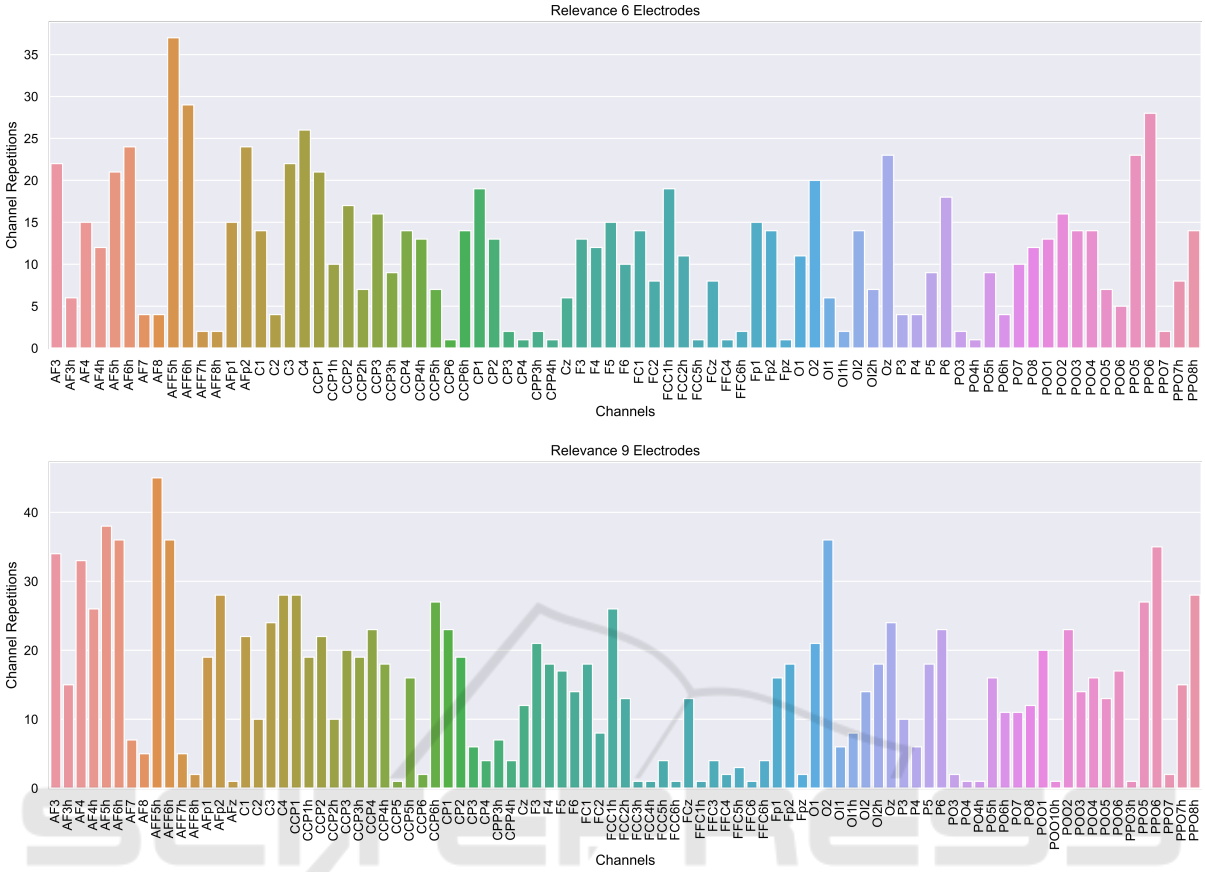

Figure 7: Channel repetition for relevance-based selection.

sponses should be done in order to validate the proposed selection over a more realistic scenario. However, the presented framework for source and EEG simulation in this study simulates signals with similarities to ERPs as can be seen in figure 1. In addition, considering that the level of noise added to the signals had equal power than the signal, the trial data simulated here can be regarded as having a similar SNR to typical ERP signals.

In this study, we introduced the concept of relevance for channel selection applied in specific time windows (time-ROI) in which the underlying activity was registered by the EEG recordings and compared the performance of multiple high-density electrode arrays, standard montages, and low-density versions based on coverage criterion. We can conclude that the localization accuracy and waveform of reconstructed sources with subsets of $Rel-6E$ and $Rel-9E$ relevant channels are comparable with reconstructions done with coverage-based distributed sets of $HD-128$ channels, and better than $62E(10-10)$ channel layout for a particular brain activity.

AUTHOR CONTRIBUTIONS

AS and EG conceived and designed the experiments. AS performed the experiments. AF, LL, MM discussed and selected the source reconstruction algorithms. All the authors analyzed the data, discussed teh results and wrote and refined the mansucript.

ACKNOWLEDGMENT

This work was supported by the Enabling technology program of Biotechnology of Norwegian University of Science and Technology NTNU, project ”David and Goliath: single-channel EEG unravels its power through adaptive signal analysis”.

REFERENCES

(1961). The ten twenty electrode system: International federation of societies for electroencephalography and

clinical neurophysiology. *American Journal of EEG Technology*, 1(1):13–19.

Chatrian, G. E., Lettich, E., and Nelson, P. L. (1985). Ten percent electrode system for topographic studies of spontaneous and evoked eeg activities. *American Journal of EEG Technology*, 25(2):83–92.

Colton, D. and Kress, R. (2019). *Inverse Acoustic and Electromagnetic Scattering Theory*. Springer, 4 edition.

Edelman, B. J., Baxter, B., and He, B. (2016). Eeg source imaging enhances the decoding of complex right-hand motor imagery tasks. *IEEE Transactions on Biomedical Engineering*, 63:4–14.

Friston, K., Harrison, L., Daunizeau, J., Kiebel, S., Phillips, C., Trujillo-Barreto, N., Henson, R., Flandin, G., and Mattout, J. (2008). Multiple sparse priors for the M/EEG inverse problem. *NeuroImage*, 39(3):1104–1120.

Gramann, K., Gwin, J. T., Ferris, D. P., Oie, K., Jung, T.-P., Lin, C.-T., Liao, L.-D., and Makeig, S. (2011). Cognition in action: imaging brain/body dynamics in mobile humans. 22(6):593–608.

Hallez, H., Vanrumste, B., Grech, R., Muscat, J., De Clercq, W., Vergult, A., D'Asseler, Y., Camilleri, K. P., Fabri, S. G., Van Huffel, S., and Lemahieu, I. (2007). Review on solving the forward problem in EEG source analysis. *Journal of NeuroEngineering and Rehabilitation*, 4.

Hämäläinen, M. S. and Ilmoniemi, R. J. (1994). Interpreting magnetic fields of the brain: minimum norm estimates. *Medical & Biological Engineering & Computing*, 32(1):35–42.

Huang, Y., Parra, L. C., and Haufe, S. (2016). The new york head—a precise standardized volume conductor model for eeg source localization and tes targeting. *NeuroImage*, 140:150 – 162. Transcranial electric stimulation (tES) and Neuroimaging.

Ilmoniemi, R. J. and Sarvas, J. (2019). *Brain Signals: Physics and Mathematics of MEG and EEG*. The MIT Press.

Iwaki, S. and Ueno, S. (1998). Weighted minimum-norm source estimation of magnetoencephalography utilizing the temporal information of the measured data. *Journal of Applied Physics*, 83(11):6441.

Jasper, H. (1958). Ten-Twenty Electrode System of the International Federation. *Electroencephalography and Clinical Neurophysiology*, 10:371–375.

Jatoi, M. A. and Kamel, N. (2018). Brain source localization using reduced eeg sensors. *Signal, Image and Video Processing*, 12(8):1447–1454.

Jatoi, M. A., Kamel, N., Malik, A. S., Faye, I., and Begum, T. (2014). A survey of methods used for source localization using eeg signals. *Biomedical Signal Processing and Control*, 11:42 – 52.

Lau-Zhu, A., Lau, M. P., and McLoughlin, G. (2019). Mobile EEG in research on neurodevelopmental disorders: Opportunities and challenges. *Developmental Cognitive Neuroscience*, 36:100635.

Lindgren, J. T. (2017). As above, so below? Towards understanding inverse models in BCI. *Journal of Neural Engineering*, 15(1):012001.

Mäkelä, N., Stenroos, M., Sarvas, J., and Ilmoniemi, R. J. (2018). Truncated RAP-MUSIC (TRAP-MUSIC) for MEG and EEG source localization. *NeuroImage*, 167:73–83.

Michel, C. M. and Brunet, D. (2019). EEG source imaging: A practical review of the analysis steps. *Frontiers in Neurology*, 10(APR):325.

Mosher, J. C. and Leahy, R. M. (1998). Recursive MUSIC: A framework for EEG and MEG source localization. *IEEE Transactions on Biomedical Engineering*, 45(11):1342–1354.

O'Leary, J. (1970). Hans berger on the electroencephalogram of man. the fourteen original reports on the human electroencephalogram. translated from the german and edited by pierre gloor. *Science*, 168:562–563.

Oostenveld, R. and Praamstra, P. (2001). The five percent electrode system for high-resolution EEG and ERP measurements. *Clinical Neurophysiology*, 112(4):713–719.

Pascual-Marqui, R. D. (2002). Standardized low-resolution brain electromagnetic tomography (sLORETA): Technical details. *Methods and Findings in Experimental and Clinical Pharmacology*, 24(SUPPL. D):5–12.

Phillips, J. W., Leahy, R. M., Mosher, J. C., and Timsari, B. (1997). Imaging neural activity using MEG and EEG. *IEEE Engineering in Medicine and Biology Magazine*, 16(3):34–42.

Seeck, M., Koessler, L., Bast, T., Leijten, F., Michel, C., Baumgartner, C., He, B., and Beniczky, S. (2017). The standardized EEG electrode array of the IFCN.

Sohrabpour, A., Lu, Y., Kankirawatana, P., Blount, J., Kim, H., and He, B. (2015). Effect of EEG electrode number on epileptic source localization in pediatric patients. *Clinical Neurophysiology*, 126(3):472–480.

Soler, A., Giraldo, E., and Molinas, M. (2020a). Low-density EEG for Source Activity Reconstruction using Partial Brain Models. In *Proceedings of the 13th International Joint Conference on Biomedical Engineering Systems and Technologies*, pages 54–63. SCITEPRESS - Science and Technology Publications.

Soler, A., Muñoz-Gutiérrez, P. A., Bueno-López, M., Giraldo, E., and Molinas, M. (2020b). Low-Density EEG for Neural Activity Reconstruction Using Multivariate Empirical Mode Decomposition. *Frontiers in Neuroscience*, 14:175.

Song, J., Davey, C., Poulsen, C., Luu, P., Turovets, S., Anderson, E., Li, K., and Tucker, D. (2015). EEG source localization: Sensor density and head surface coverage. *Journal of Neuroscience Methods*, 256:9–21.

Wolf, L. and Shashua, A. (2005). Feature Selection for Unsupervised and Supervised Inference: The Emergence of Sparsity in a Weight-Based Approach * Amnon Shashua. *Journal of Machine Learning Research*, 6:1855–1887.